International Journal of Rock Mechanics & Mining Sciences 75 (2015) 233–243

Contents lists available at ScienceDirect

International Journal of Rock Mechanics & Mining Sciences

journal homepage: www.elsevier.com/locate/ijrmms

Estimating tunnel wall displacements using a simple sensor based on a Brillouin optical time domain reflectometer apparatus

Ricardo Moffat, Javier Sotomayor, Juan Felipe Beltrán *

Department of Civil Engineering, University of Chile, Santiago, Chile

ARTICLE INFO

Article history:
Received 28 January 2014
Received in revised form
9 October 2014
Accepted 16 October 2014
Available online 7 March 2015

Keywords:
BOTDR
Optical fiber
Strain gauge
Field monitoring
Back-analysis
Deformation

ABSTRACT

A strain monitoring system based on a PVC tube instrumented with optical fiber connected to a Brillouin Optical Time Domain Reflectometer (BOTDR) apparatus is proposed to monitor rock mass movement in an underground mine. The optical fiber is glued along four lines of the tube surface which are rotated 90° one from each other to capture in-plane and out-of-plane tube bending displacements. A laboratory experimental program is undertaken to validate the proposed sensor as a monitoring tool. In the laboratory, PVC tubes are subjected to controlled displacements on 4 points that represent the attachment locations of the sensor to the rock mass to simulate possible response in the rock mass during mining activities. The longitudinal strain recorded by the optical fiber compare well with the ones provided by the traditional electrical resistance strain gauges. Considering the sensor tube as a one-dimensional linear beam-type element, a back-analysis algorithm is implemented to estimate displacements on the surface of the rock mass using the recorded longitudinal strains. The proposed sensor is installed in a tunnel mine and preliminary strain measurements of this field trial are reported. The conclusions of this study suggest that the proposed sensor can be regarded as a promising and safe tool for tunnel monitoring.

1. Introduction

Monitoring strain in structures such as bridges, tunnels, pipelines, and buildings are important for disaster prevention, detecting the deterioration of structures, and reducing the repair and maintenance cost of structural members [1–3]. In particular, tunnel excavation in rocks induces changes in the local stress field and subsequent deformation; thus the purpose of the instrumentation of the tunnel walls is to monitor displacement in order to maintain safe operational practices, evaluate the stability, and measure rock mass properties. In addition to the complexity of the analysis of possible failure mechanisms, rock, as a natural material, is heterogeneous and difficult to characterize completely. In order to avoid large displacement and failure inside underground mines, geotechnical engineers consider stress, seismicity, and displacement measurements. In situ field monitoring is therefore essential to decrease the probability of failure and perform mining activities safely.

Deformation in underground structures are usually monitored by recording the displacements of a limited number of carefully selected points allowing the key warning signs of instability to be appropriately monitored. Borehole extensometers and inclinometers are commonly used in underground measurements [4–6]. Their use, however, frequently requires a data acquisition system close to the zone that is being monitored increasing the risk of the workers who are taking the measurements. In the last years, geodesy has offered an alternative technology suitable for such applications in which a large number of control points are considered. Electronic theodolites have been used to monitor induced deformation during tunnel excavation in which the data collected can describe 3-D changes of the tunnel walls and compare them with the expected values to check the safety of the tunnel excavation [7,8]. Geodesic instruments, however, require regular cleaning regime to ensure that they are working properly due to their exposure to demanding working environment (dust and humidity) usually encountered during excavation works and mining activities.

Strain measurements with a distributed Brillouin scattering based sensor system appear to be a promising alternative for the health monitoring of civil structures as explained in [9]. The BOTDR-based fiber optic technique can provide a distributed measurement of physical parameters of structures over a long distance. For Brillouin-based optical sensing, the entire length of fiber optic cables is used for both data transmission and strain

* Corresponding author. Tel.: +56 2 29784929.
E-mail address: jbeltran@ing.uchile.cl (J.F. Beltrán).

http://dx.doi.org/10.1016/j.ijrmms.2014.10.013
1365-1609/

sensing. As such, using the BOTDR technique makes it possible to measure the strain continuously (every 5 cm) along the fiber optic cable rather than at discrete points, with a spatial resolution that can be varied. Fiber optic sensors based on Brillouin scattering make use of a nonlinear interaction between the light and the silica material of which the fiber is made. If light pulses are transmitted down a fiber, part of the pulse is scattered back at every point along the fiber. The scattered light experiences a frequency shift that depends on the fiber temperature and strain (i.e., local properties of the fiber). A system based on this type of sensing is a useful tool for structural and health monitoring of underground structures [10–13].

Optical fiber sensors have many advantages over other measurement systems such as immunity to electromagnetic interference, being lightweight and small size, and low power. A large number of sensors can be monitored at the same time from one acquisition data equipment, as well as the fact that equipment and personnel can be at a long distance from the monitored area thus improving safety as mentioned in [14–16]. In this context, optical fiber sensors appear to be a promising alternative to monitor rock mass displacements during mining activities.

In this study a strain sensor based on the BOTDR technique is proposed to estimate rock mass displacements from longitudinal strain measurements. The proposed instrument consists of a polyvinyl chloride (PVC) tube instrumented with Brillouin fiber optic sensor along its external surface. This sensor is validated in the laboratory by comparing the recorded longitudinal strain measures with the strain measured by electrical resistance strain gauges. The installation of the sensor in a underground mine, preliminary sensor readings, and a back-analysis procedure implemented to utilize the longitudinal strains measured by the sensor to estimate rock mass displacements at the interior of a tunnel due to operational mining activities are presented and discussed in this paper.

2. BOTDR optical fiber sensor description

PVC tubes of 5.0 m length, 25 mm and 40 mm external diameter, and 2 mm and 3 mm of thickness, respectively, were used to create the strain sensors. Standard properties of the PVC are: rupture tensile stress equal to 500 kg/cm^2, elasticity modulus of 30,000 kg/cm^2, and axial failure strain equal to 15% [17]. Strains along the PVC tube are measured using the BOTDR equipment where the optical fiber is located on the PVC tubes surfaces as shown in Fig. 1. The sensing fiber is nylon coated standard single-mode optical fiber with a diameter of 0.9 mm. It is glued to the PVC tubes by the use of epoxy glue applying an initial tensile force that approximately corresponds to a strain of about 0.1%. There are four lines of sensor fiber; upper ($z=0$, $y=d/2$), bottom ($z=0$, $y=-d/2$), left ($z=d/2$, $y=0$), and right ($z=-d/2$, $y=0$) and 3 loops between them (Fig. 2(a)). These loops are approximately 0.5 m length to avoid large signal losses. No compensation of temperature was applied as it was verified that changes in temperature during testing were lower than the error (i.e., 0.01%) given by the fabricant of the BOTDR equipment and verified in a experimental program [18] (however this compensation should be considered in the mine for long term measurements). These PVC tubes are also instrumented with 30 mm long electrical resistance strain gauges for validation purposes. Strain gauges give local measurements of longitudinal strain on the upper, lower and a lateral face of the PVC tubes, providing a strain resolution of 0.01% (PFL-20-11, TML). Strain gauges were installed slightly rotated relative to the optical fiber as depicted in Fig. 2a and their distributions along the length

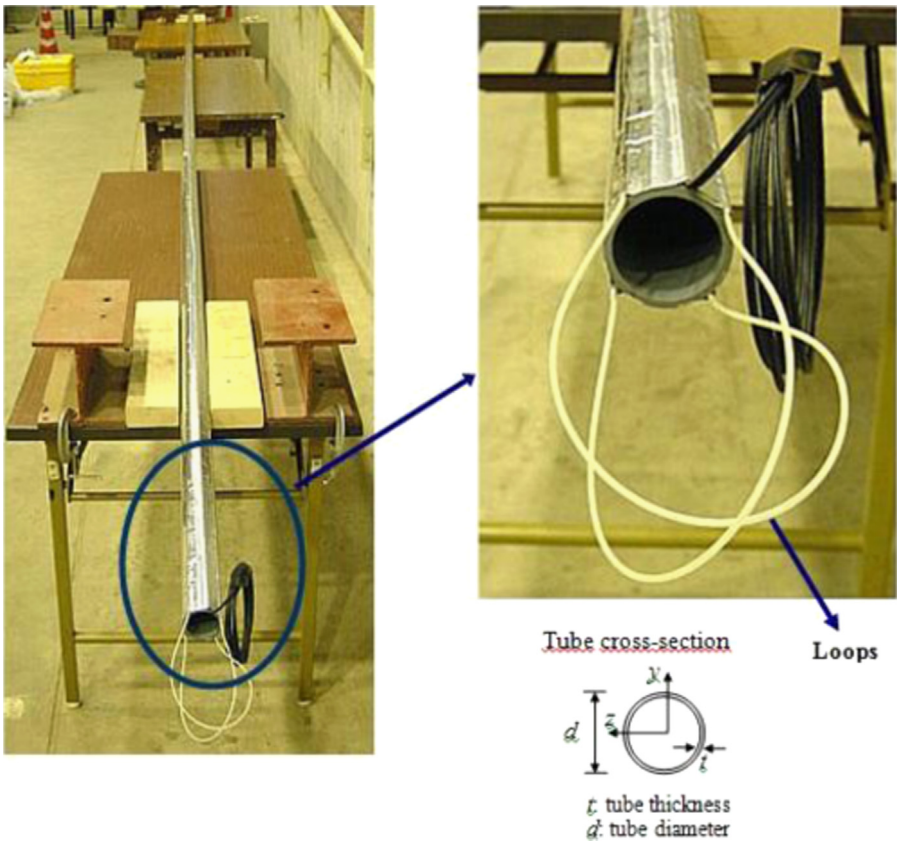

Fig. 1. PVC tube instrumented with optical fiber.

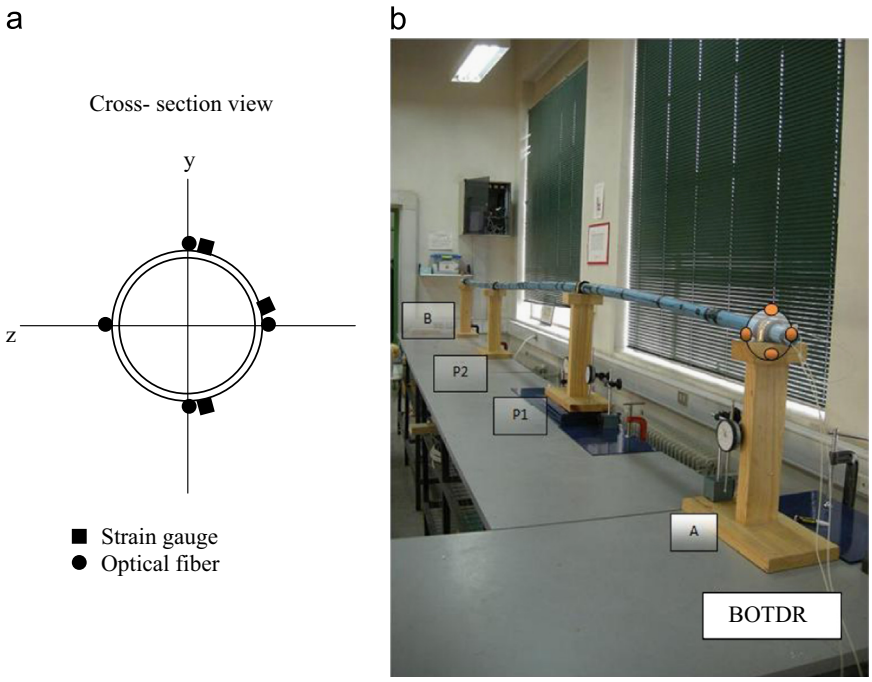

Fig. 2. (a) Distribution of the optical fiber and strain gauges on the tube cross-section; (and b) sensor tube supports: B, P2, P1, and A.

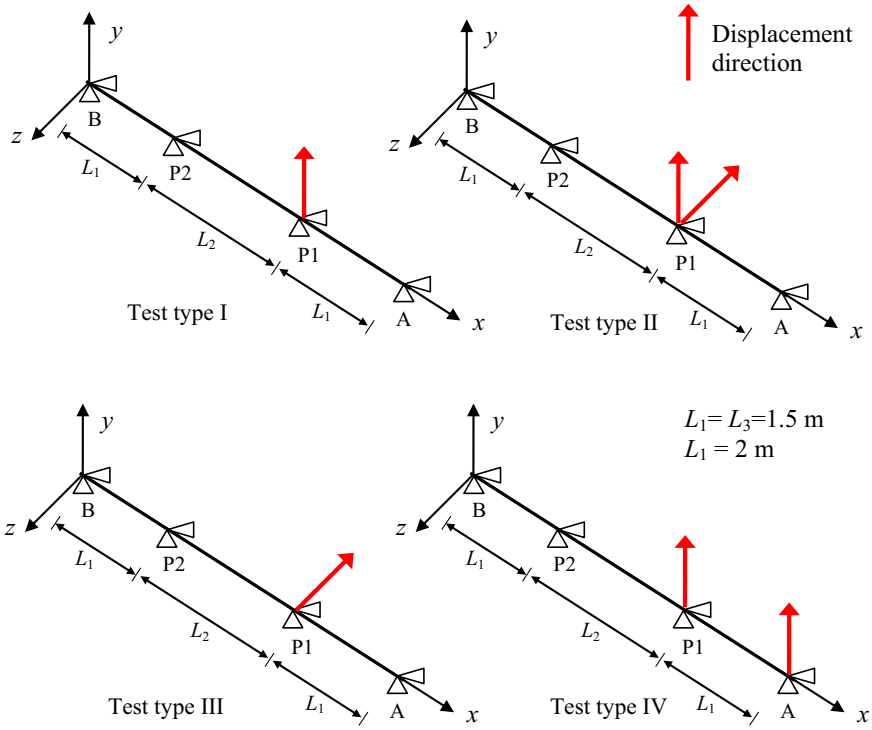

Fig. 3. Sketch of the Types of laboratory test performed.

of the tubes are shown in the figures in which the experimental validation of the proposed sensor is presented.

The sensor tube (ST) is supported in four points: A, B, P1, and P2 (Fig. 2(b)) which represent the attachment locations of the sensor to the rock mass in the field. The installation distance from A to P1 and from P2 to B is equal to 1.5 m and from P1 to P2 is equal to 2 m. These supports are materialized by wood pedestals over which the ST is fixed using metal clamps. The optical fiber is prevented from damage as the clamps are tied by using rubber sheets between the fiber and the clamps. The ST is designed to measure longitudinal strain due to relative displacements of its supports which are rigidly connected to the rock mass. As such, if the ST is installed in a region where the rock mass locally displaces (within ST length), relative displacements of ST supports are induced due to their rigid connections to the rock mass and consequently the ST is deformed in bending. Hence, four types of controlled relative displacements are applied to ST supports during laboratory testing which are believed to characterize the most likely rock mass movements due to mining operations. The displacements of the sensor supports were monotonically applied

until a noticeable bending deformation of the PVC tubes was observed, during which the axial strains were measured using strain gauges and the BOTDR equipment. A description of the prescribed relative ST supports displacements is presented below (Fig. 3)

Type I: vertical (in plane) displacement of point P1.
Type II: vertical and horizontal (out of plane) displacement of point P1.
Type III: horizontal displacement of point P1.
Type IV: vertical displacement of points A and P1.

3. Laboratory tests

In total, eighteen laboratory tests were performed during this study on tubes of length equal to 5.0 m. Half of these tests were carried out on 40 mm external diameter tubes and the other half on 25 mm diameter tubes. The 40 mm diameter tube was chosen to construct the proposed optical fiber sensor employed underground because the sensor is designed for long-term monitoring and a 40 mm diameter tube develops greater axial strain than a 25 diameter tube for the same displacement as discussed later in the paper. Thus, smaller strain of the rock mass can be properly detected (i.e., axial strain values greater than the error of the optical fiber) using the larger diameter tube. In order to avoid repeated analyses and present concise conclusions of the study carried out, only the results associated to the 40 mm diameter tube sensor are discussed in detail throughout this paper. Comments on the results obtained for the 25 mm diameter tube, however, are provided as needed.

Total strains values are recorded directly by the BOTDR equipment. Net strains are calculated by subtracting to each recorded measurement the strain values recorded in the original configuration of the ST (i.e., before deformation due to prescribed supports displacements). Net strain values are then used to estimate the displacements at support points as will be discussed later in Section 4 (Back-analysis algorithm).

Comparisons of the measured strains values induced by the supports movements associated to the tests types previously described using both the BOTDR and electrical resistance strain

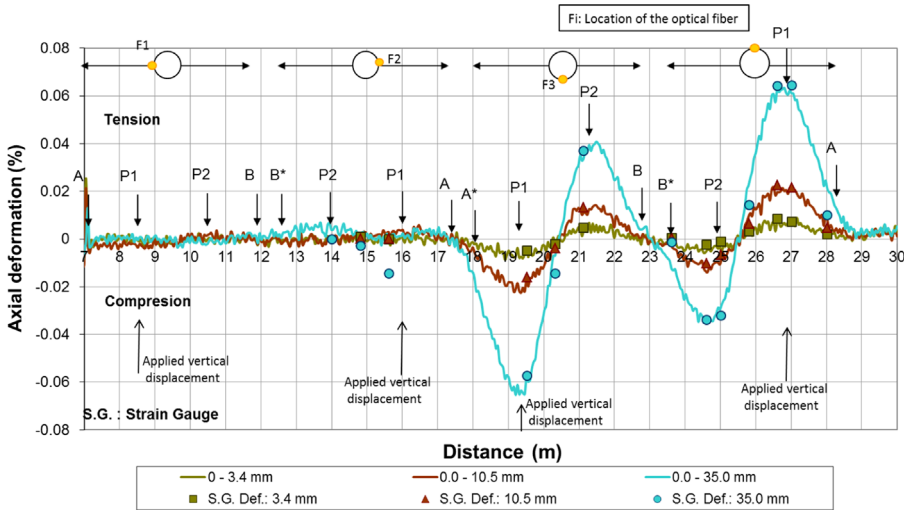

Fig. 4. Comparisons net strain measurements test Type I.

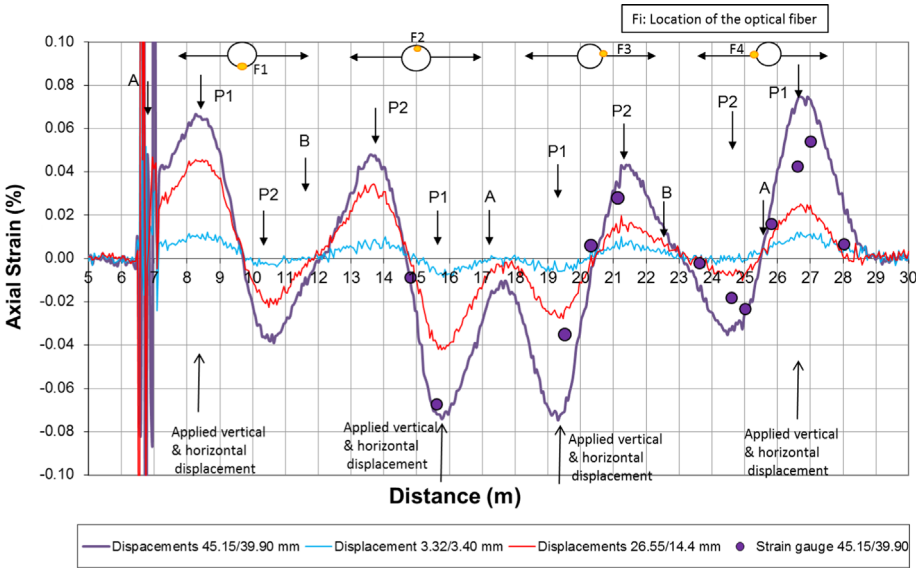

Fig. 5. Comparisons net strain measurements test Type II.

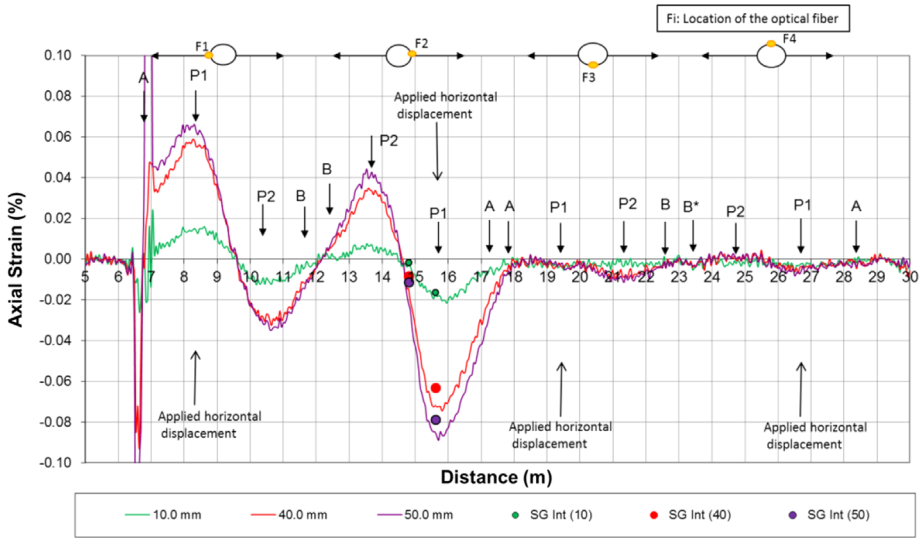

Fig. 6. Comparisons net strain measurements test Type III.

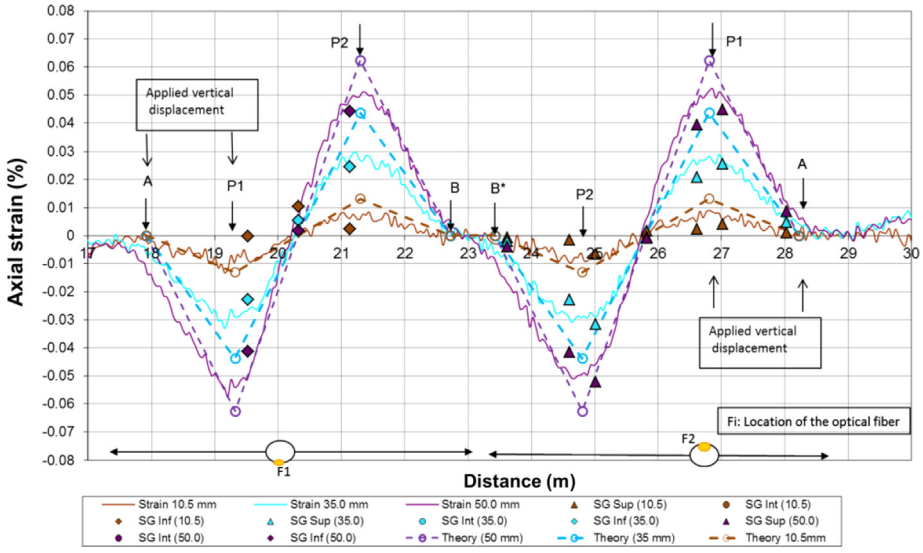

Fig. 7. Comparisons net strain measurements test Type IV.

gauges are presented from Figs. 4–7. Similar strain distribution patters along the ST are obtained for the same type of prescribed supports displacement differing them in the magnitude of the strain values recorded: greater supports displacements induce greater axial strain values in the ST as shown from Fig. 4 to Fig. 7. This difference in the observed axial strain values for each type of supports movement, is the key feature to back-analyze the measured strains and estimate the displacements of the supports points (A, B, P1, and P2). In Fig. 4, vertical displacement of point P1 ranges from 3.4 mm to 35 mm (Test type I). The maximum axial strain is equal to 0.062%, which is much lower than the elastic strain limit of the fiber (1%) according to [18]. The plots also show that displacements in the y (vertical) direction do not induce axial strains at $z=\pm d/2$ (horizontal) locations; thus axis z–z is the neutral axis for displacements in the y direction (Fig. 1). The same conclusions are drawn for the results given by the type III tests for a horizontal displacement of point P1 that ranges from 10 mm to 40 mm (Fig. 6): fiber has an elastic behavior because the maximum axial strain recorded is equal to 0.082% which is lower than the elastic strain limit of the fiber (1%) and horizontal displacements (z direction) do not induce axial strain at $y=\pm d/2$ locations; thus axis y–y is the neutral axis for displacements in the z direction.

The measured net axial strains associated with the Test type II are presented in Fig. 5. This test combines the vertical and horizontal displacements of point P1; hence the ST recorded strain measurements along its entire length in which the range of variation of the specified displacements were [3.32, 45.15] mm and [3.4, 39.9] mm in the y and z directions respectively as depicted in Fig. 5. Based on the ST structural behavior under tests type I and type III (Figs. 4 and 6) in which vertical (y axis) and horizontal (z axis) displacements are uncoupled having the ST only in plane deformation, it can be concluded that the ST is capable of measuring strains due to a combination of vertical and horizontal displacements. The maximum strain value measured was equal to 0.057% for a prescribed vertical displacement equal to 50.0 mm, value that is lower than the elastic strain limit of the fiber.

Test type IV considers the relative movement of two ST adjacent supports in the vertical plane (y direction). The ST deforms only in the vertical plane in which its cross-section rotates around the z–z axis. Axial strains are measured by the optical fiber at $y=\pm d/2$ locations as depicted in Fig. 7 for equal

displacements of the A and P1 supports that range from 10.5 mm to 50.0 mm. Accordingly, null axial strains were measured at $z=\pm d/2$ locations and thus only the axial strain measured at $y=\pm d/2$ is shown in Fig. 7.

Based on the results presented from Figs. 4–7, it can be observed that there is a good agreement between the measurements from both BOTDR and electrical resistance gauges in which the differences among them are in the expected error of both measurement techniques (0.01%) according to [18]. Some differences among them, however, were expected due to the different locations on tubes cross-section that these two sensors were placed (Fig. 2(a)). There is more scatter, especially near the ST supports, between the strain measurement for test types II and IV in which the strain values obtained from the electrical resistance gauges are lower than the strain values measured by the optical fiber which is in accordance with the fact that the electrical resistance gauges were installed closer to the neutral axis of the tubes. One of the possible explanation of this higher scatter is that Test types II and IV involve more complicated tube deformation process than Test types I and III which may induce rapid changes in strain distribution near the tubes supports (locations where prescribed displacements are defined and where scatter among data is bigger) that is not accurately measured by the optical fiber as discussed in [18,19].

Strain distributions measured from the four laboratory tests types considered in this study have similar results: the gradient strain values change at ST supports (strains peaks) and the distribution of measured strain values between these strains peaks can be accurately approximated by a linear curve, except in the vicinity of the sensor supports (see Fig. 7). Axial strain theoretically estimated by considering the ST as one-dimensional linear structural member (deformable Bernoulli beam element) subjected to relative displacement, compare well with measured values for the regions between sensor supports (points A, B, P1 and P2) except in the vicinity of the supports where theoretical values deviate from measured values due to the Saint Venant's principle [20]. In this particular application, this principle establishes that the reaction forces developed at the ST supports locally affect (i.e., near the sensor supports) the stress and strain distributions given by linear beam theory. The results given by test type IV was selected for the analysis because its associated ST deformed configuration can be represented as a linear combination of the deformed configurations of test types I, II, and III provided that strains induced by vertical and horizontal displacements are uncoupled. Thus, for the range of support displacements used in this experimental study, because linear beam theory estimates in a satisfactory manner strain distributions associated to the Test type IV (Fig. 7), strain distributions associated to Test types I, II, and III are also well predicted by this linear theory. Details of how the linear Bernoulli beam theory is used to estimate relative ST support displacements based on the distribution of axial strain measured along the ST length is explained in detail in the following section.

4. Back-analysis algorithm

4.1. Description of the algorithm

As explained in Section 1, axial strains are continuously measured by the BOTDR along the PVC tube at opposite positions of its circumference as indicated in Fig. 1. Accordingly, the BOTDR optical fiber sensor is used to monitor deformation in tunnels due to relative transverse displacements of the rock mass. A simple analysis, based on the linear theory of strength of materials and considering the PVC tube as deformable structural element, can be performed to estimate the rock mass movements that cause the strain recorded by the sensor.

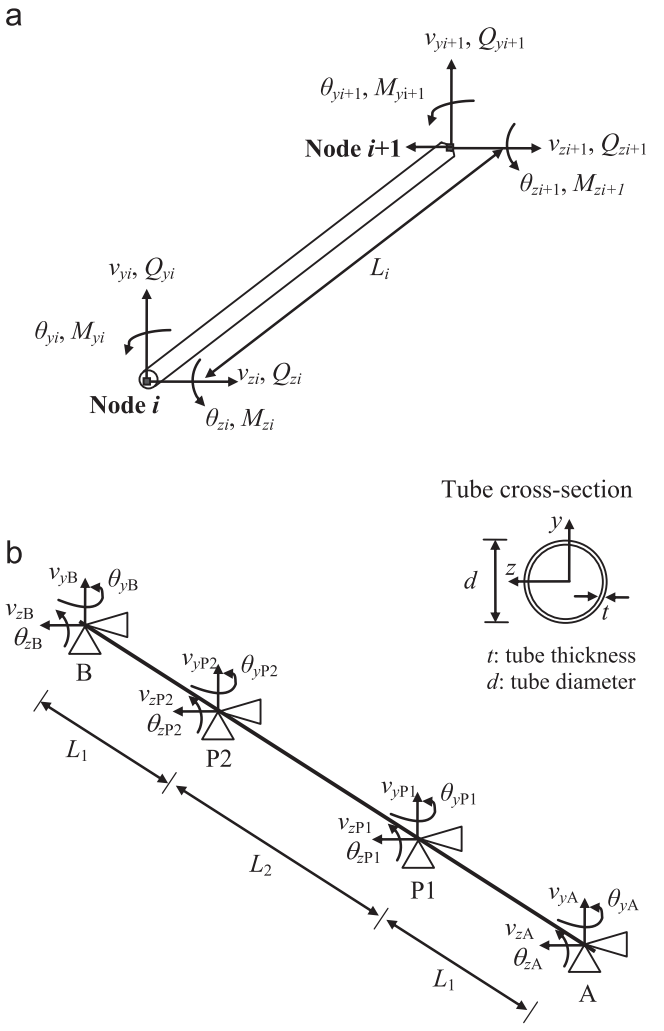

Fig. 8. (a) Degrees of freedom of a beam-element and (b) structural modeling of an ST.

In order to model a PVC tube as a deformable structural element, the following assumptions are made: (1) PVC has a linear-elastic uniaxial stress–strain curve; (2) small deformation-based formulation is assumed to be valid; and (3) weight of the tube is considered to be negligible [20,21]. The ST is discretized into three two-noded linear beam elements. Each beam element i (Fig. 8(a)) includes four degrees of freedom at each node: transverse displacements ($v_{\eta i}$, $v_{\xi i}$) and bending rotations ($\theta_{\eta i}$, $\theta_{\xi i}$) where η and ξ correspond to perpendicular local axes. Associated with these local degrees of freedom are the corresponding shear forces $Q_{\eta i}$ and $Q_{\xi i}$, and bending moments $M_{\eta i}$ and $M_{\xi i}$ respectively, variables related each other through the beam element stiffness matrix as presented in the following equation:

$$\begin{bmatrix} \frac{12EI_z}{L_i^3} & 0 & 0 & \frac{6EI_z}{L_i^2} & -\frac{12EI_z}{L_i^3} & 0 & 0 & \frac{6EI_z}{L_i^2} \\ 0 & \frac{12EI_\eta}{L_i^3} & \frac{6EI_\eta}{L_i^2} & 0 & 0 & -\frac{12EI_\eta}{L_i^3} & \frac{6EI_\eta}{L_i^2} & 0 \\ 0 & \frac{6EI_\eta}{L_i^2} & \frac{4EI_\eta}{L_i} & 0 & 0 & -\frac{6EI_\eta}{L_i^2} & \frac{2EI_\eta}{L_i} & 0 \\ \frac{6EI_z}{L_i^2} & 0 & 0 & \frac{4EI_z}{L_i} & -\frac{6EI_z}{L_i^2} & 0 & 0 & \frac{2EI_z}{L_i} \\ -\frac{12EI_z}{L_i^3} & 0 & 0 & -\frac{6EI_z}{L_i^2} & \frac{12EI_z}{L_i^3} & 0 & 0 & -\frac{6EI_z}{L_i^2} \\ 0 & -\frac{12EI_\eta}{L_i^3} & -\frac{6EI_\eta}{L_i^2} & 0 & 0 & \frac{12EI_\eta}{L_i^3} & -\frac{6EI_\eta}{L_i^2} & 0 \\ 0 & \frac{6EI_\eta}{L_i^2} & \frac{2EI_\eta}{L_i} & 0 & 0 & -\frac{6EI_\eta}{L_i^2} & \frac{4EI_\eta}{L_i} & 0 \\ \frac{6EI_z}{L_i^2} & 0 & 0 & \frac{2EI_z}{L_i} & -\frac{6EI_z}{L_i^2} & 0 & 0 & \frac{4EI_z}{L_i} \end{bmatrix} \begin{Bmatrix} v_{\eta 1} \\ v_{\xi 1} \\ \theta_{\eta 1} \\ \theta_{\xi 1} \\ v_{\eta 2} \\ v_{\xi 2} \\ \theta_{\eta 2} \\ \theta_{\xi 2} \end{Bmatrix} = \begin{Bmatrix} Q_{\eta 1} \\ Q_{\xi 1} \\ M_{\eta 1} \\ M_{\xi 1} \\ Q_{\eta 2} \\ Q_{\xi 2} \\ M_{\eta 2} \\ M_{\xi 2} \end{Bmatrix} \quad (1)$$

where E is the Young's modulus of the PVC; and I_ξ and I_η are the inertias with respect to the ξ-ξ and η–η principal axes; and L_i is the length of the ith beam element. The external actions that induce axial strains in the PVC tube are the relative displacements of the PVC tube supports which represent the relative transverse displacements of the rock mass.

The deformed configuration of the PVC tube is completely determined if the degrees of freedom previously defined (Fig. 8(a)) are known. Using a standard structural analysis procedure [21], the three two-noded beam elements are assembled to obtain a discrete model for the ST (Fig. 8(b)). This model leads to represent the equilibrium of the system by a set of linear equations that in matrix form can be written by

$$[K]\{u\} = \{R\} \tag{2}$$

where $[K]$ denotes the stiffness matrix of the ST, $\{u\}$ is the displacements and rotations vector (degrees of freedom), and $\{R\}$ is the nodal load vector. In this particular application, the local beam element axes (η,ξ) coincide with the global coordinate system (y, z) as shown in Fig. 8(b). It is assumed that stress in the rock mass induces both vertical (y direction) and horizontal (z direction) displacements relative to the sensor supports; thus, the only nonzero components of the nodal load vector $\{R\}$ are the shear forces related to the prescribed sensor supports displacements [21].

Axes z–z and y–y (Fig. 8b) are the neutral axes (zero axial strain) for the bending moments around z–z (associated to a displacement in y direction) and y–y (associated to a displacement in z direction) respectively. Thus, strains measured at $z=\pm d/2$ are solely related to horizontal displacements (z-direction) and strains at $y=\pm d/2$ are solely related to vertical displacements (y-direction). Using the theoretical model, the axial strains recorded by the sensors (in-situ and/or during experimental tests) can be back-analyzed to estimate the relative displacement of the sensors supports and thus monitor in situ strain in a rock mass.

In linear structural analysis, support displacements induce linear axial strain distribution along the structural element; hence for computational purposes of the proposed back-analysis algorithm, the best-fit linear curves are computed to the input data considering those at a distance $5d$*(d is the tube diameter)* away from the sensor supports to avoid the nonlinearities presented in these zones according to the Saint Venant's principle and the fact that optical fiber does not accurately measure strains near singularities (i.e., sensor supports) as previously discussed. The developed back-analysis algorithm is based on the minimization of an error function representing the difference between the measured axial strain distribution (field or laboratory) along the length of the sensor and their estimated values using the aforementioned structural model of the sensor. This algorithm proceeds with the following steps:

Step 1: Axial strain distributions $\varepsilon(x)$ along the sensor at locations $y=\pm d/2$ and $z=\pm d/2$ of its cross-section, measured in-situ or laboratory, are the input data (see Fig. 8(b)). Best-fit linear curves are computed to these data and bending moment diagrams M_z and M_y are computed based upon the data from these curves (variable ε) at $y=\pm d/2$ and $z=\pm d/2$ respectively, as follows [20]:

$$M(x) = \left(\pm\frac{2}{d}\right) EI\varepsilon(x) \tag{3}$$

Step 2: Shear forces at each node of the beam elements are computed using the following equilibrium equation:

$$Q_{yk,k} = \frac{M_{yk,k}+M_{yk,k+1}}{L_k} = -Q_{yk,k+1} \tag{4}$$

$$Q_{zk,k} = \frac{M_{zk,k}+M_{zk,k+1}}{L_k} = -Q_{zk,k+1} \tag{5}$$

where the first and second k subscripts of the variables Q and M refer to the kth beam element and to node (k and $k+1$) of the that element respectively; L_k is the length of the kth beam element (Fig. 8(b)). Shear forces in the y direction are associated to bending moment M_z and shear forces in the z direction to bending moment M_y (Fig. 8(a)).

Step 3: Assume a displacement sensor of the supports (for the sake of the discussion the subscript m is used to identify a particular type of displacement supports) and obtain the nonzero jth components of the nodal load vector $\{R\}$ from the following general equilibrium equation

$$R_{jm} = V_{(j-1,j)m} + V_{(j,j)m} \tag{6}$$

where the variable $V_{k,l}$ refers to the contribution of the kth element ($k=1,2$, and 3) to the shear force related to the lth degree of freedom (displacement) of the sensor. This shear force R_j could be in the y or z direction (Q_y or Q_z) depending on from which optical fiber input data for algorithm is obtained as previously discussed.

Step 4: Solve the system of equations represented by Eq. (2) for the assumed unknown degrees of freedom of the sensor.

Step 5: For the kth ($k=1,2$, and 3) beam element that forms the sensor, compute its transverse displacement based on the following relationship:

$$\begin{Bmatrix} v_k(x) \\ w_k(x) \end{Bmatrix}_m = \begin{bmatrix} N_1(x) & 0 & N_2(x) & 0 & N_3(x) & 0 & N_4(x) & 0 \\ 0 & N_1(x) & 0 & N_2(x) & 0 & N_3(x) & 0 & N_4(x) \end{bmatrix} \times \begin{Bmatrix} v_k \\ w_k \\ \varphi_k \\ \theta_k \\ \vdots \\ \theta_{k+1} \end{Bmatrix}_m \tag{7}$$

where the functions $N_i(x)$ are the so-called 1D shape functions which are used for interpolation of $v(x)_m$ and $w(x)_m$ using their nodal values (degrees of freedom). The 1D shape functions for a two-noded beam element are given by [21]

$$N_1 = 1 - 3\left(\frac{x}{L}\right)^2 + 2\left(\frac{x}{L}\right)^3 \tag{8}$$

$$N_2 = x\left(1-\frac{x}{L}\right)^2 \tag{9}$$

$$N_3 = 3\left(\frac{x}{L}\right)^2 - 2\left(\frac{x}{L}\right)^3 \tag{10}$$

$$N_4 = x\left[\left(\frac{x}{L}\right)^2 - \frac{x}{L}\right] \tag{11}$$

where the variables x and L are the position along the longitudinal axis and length of the beam element respectively.

Step 6: Compute the curvatures (both planes) for the kth ($k=1,2$, and 3) beam element of the sensor using the following simplified expressions:

$$(\phi_{zz})_{km} = \left(\frac{d^2 v_k}{dx^2}\right)_m ; \quad (\phi_{yy})_{km} = \left(\frac{d^2 w_k}{dx^2}\right)_m \tag{12}$$

where ϕ_{zz} and ϕ_{yy} are the curvatures in the z-plane and y-plane respectively.

Step 7: Estimate the axial strain distribution $\varepsilon_{ekm}(x)$ (the subscript m stands for the mth potential sensor supports movement) along each of the kth beam element that forms the sensor at four locations (values of the coordinates z, y): $(0,d/2)$, $(0, -d/2)$, $(d/2, 0)$, and $(-d/2, 0)$ (Fig. 8b) by

$$\varepsilon_{ekm}(x) = -(\phi_{zz})_{km}(x)y + (\phi_{yy})_{km}(x)z \tag{13}$$

Step 8: Compute the error index Err_m, associated to the mth potential sensor supports movement, defined as

$$Err_m = \left(\sum_{k=1}^{3} err_k \right)_m \tag{14}$$

$$err_{km} = \frac{1}{n_k} \sum_{t=1}^{n_k} \left| \varepsilon(x_t) - \varepsilon_{ekm}(x_t) \right| \tag{15}$$

where the variable n_k is the number of samples of the measured data for the kth beam element that forms the ST. The sensor supports movement with the least error index value (i.e., $min\{Err_m\}, \forall m$) is selected as the most probably movement experienced by the rock mass.

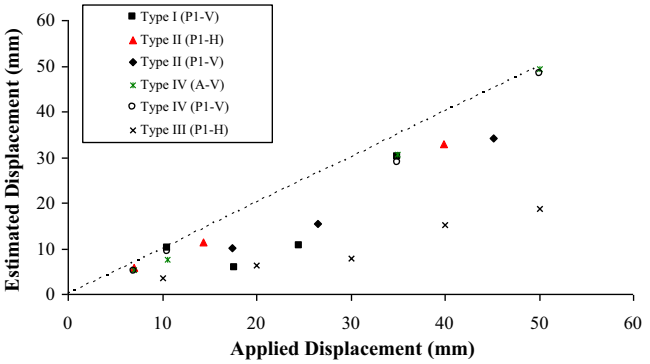

Fig. 9. Comparisons between prescribed and estimated relative supports displacements.

4.2. Validation of the algorithm

In order to validate the use of the previously described algorithm, the strain values measured by the sensors during the experimental program are back-analyzed to estimate the prescribed relative displacements of the sensors supports. The results of this comparative analysis are presented in Fig. 9 in which a 45° line (dashed line) is plotted through the origin to evaluate the accuracy of the estimated values. For each set of laboratory experimental data analyzed, the four boundary conditions specified during the experimental program (test Types I–IV) were assumed through the application of the proposed algorithm (*Step* 3). As expected, the implemented back-analysis algorithm cannot guarantee the uniqueness of the solution (i.e., relative sensor support displacements) because an acceptable agreement between the analytical results and measured data (i.e., minimization of the objective error function) may be achieved through multiple relative sensor support displacements combinations [22,23];thus the data shown in Fig. 9 correspond to the sensor supports displacements that had the least value of the error index (*Step* 8) which coincide with the boundary conditions specified during the experimental program for each set of the data analyzed.

In general, all the estimated support displacement values lay below the 45° line which indicates that the analytical model is stiffer than the tested sensors, i.e., smaller support displacements are needed to induce the same axial strain field in the beam

Fig. 10. Tube sensors attached to tunnel sidewall and ceiling.

elements (ST model) than in the tested sensors. Estimates of the supports displacements of Test type IV show a good correlation with the applied ones: the difference between them decreases from 25% to 2%, relative to the applied displacement values, as the value of the vertical displacement of support A and P1 increases from 7 mm to 50 mm. This conclusion can be attributed to the fact that the longitudinal strain measurement error associated to the optical fiber is constant (0.01%) and therefore its impact decreases with larger measured strains. The same conclusion is drawn for the Test types I and II but with a greater percentage of difference between estimated and applied supports displacements: 15% and 20% of difference for Tests types I and II for vertical displacements equal to 35 mm and 45 mm respectively. Conversely, estimates of supports displacements related to Test type III differ significantly from the applied ones reaching a difference of 65%. Despite this last conclusion, the proposed numerical algorithm to back-analyze ST measurements still provides a promising computational tool to monitor rock mass movements. It is important to point out that experiments associated to Test types I, II, and III were more difficult to perform than those related to Test type IV. The former experiments only considered the displacement of one inner ST support (support P1) which made difficult to keep the rest of the supports aligned, probably due to insufficient lateral and vertical supports stiffness (depending of the Test type).This supports misalignment results in a different deflected shape of the ST than that assumed by the numerical algorithm inducing additional strains which are measured by the optical fiber that are then used as input data to estimate supports relative displacement. Due to the significant deviation of the estimated relative supports displacement values from the 45° line shown in Fig. 9, it is suggested that misalignment effect had bigger impact on strain measurements during the execution of Test type III.

While the results given by the proposed back-analysis algorithm compare well with the imposed relative support displacement values of Test type IV and in less extent with the values specified for Type tests I and II, improvements—including a more accurate constitutive law of the PVC tube experimentally obtained rather than use a single elasticity modulus value specified by the manufacturer, consider the semi-rigid vertical and horizontal connection of the system PVC tube-metal clamps-rubber sheets to model sensor supports, and account for the nonlinear measured strain distribution around ST supports by refining the number of two-noded linear beam elements around these zones (i.e., the so-called *h*-type refinement)—can be incorporated to better represent ST behavior.

5. Field installation and preliminary measurements

The STs were installed in an underground mine, located close to the city of Santiago (capital city of Chile). The appearance of the STs attached to a tunnel wall is presented in Fig. 10 along with the detail of one (of the four) support points of the sensor and a loop of fiber used to compensate temperature changes as successfully used on field measurements by [11]. The attachment of the sensor to the rock is performed by using a steel bolt glued to the rock with grout obtaining a rigid and superficial connection to the rock at each support points as simulated in the setup of the laboratory tests. The same type of metal clamps used to build ST specimens was considered to connect the steel bolts to the ST in the field. The installation is relatively fast and simple but requires fusion the optical fiber in the field (between the sensor and transmitting fiber) and this can be difficult and time consuming in underground field conditions. The cost of installation would depend on local conditions; however it will be the BOTDR data acquisition and processing equipment the most expensive of all.

An example of preliminary measurements is shown in Fig. 11 where the evolution of the net strains developed by ST located in the undercut level of the mine for six different dates (from October 4 to December 25) is presented. Horizontal dashed-lines in the plot define the measurement error associated to the optical fiber (0.01%). The strain values developed by the ST increase with time in which the values recorded at the end of December are greater than the optical fiber error, especially the ones measured by the upper and bottom fiber which suggests that the ST mainly deforms in the vertical plane (*xy* plane, Fig. 8(b)) due to the assumption of bending behavior of the sensor. It is important to point out, however, that a sensor tube with greater diameter would develop higher axial strain values than the 40 mm diameter ST for the same rock mass movements due to the increase of the bending stiffness of the sensor. Thus, small rock mass movements can be appropriately detected (i.e, axial strain values greater than the error of the optical fiber) by larger diameter sensors which was verified performing numerical simulations using the back-analysis algorithm proposed in this study ([24]) and during the 25 mm diameter tube experimental program as shown in Fig. 12 considering arbitrarily, for the sake of the discussion, data from test

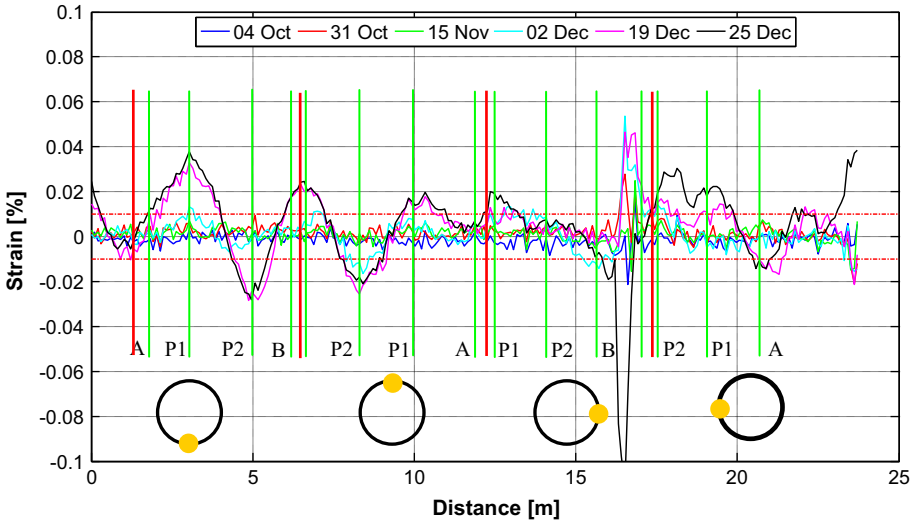

Fig. 11. Net strains developed by the tube sensor in the undercut level.

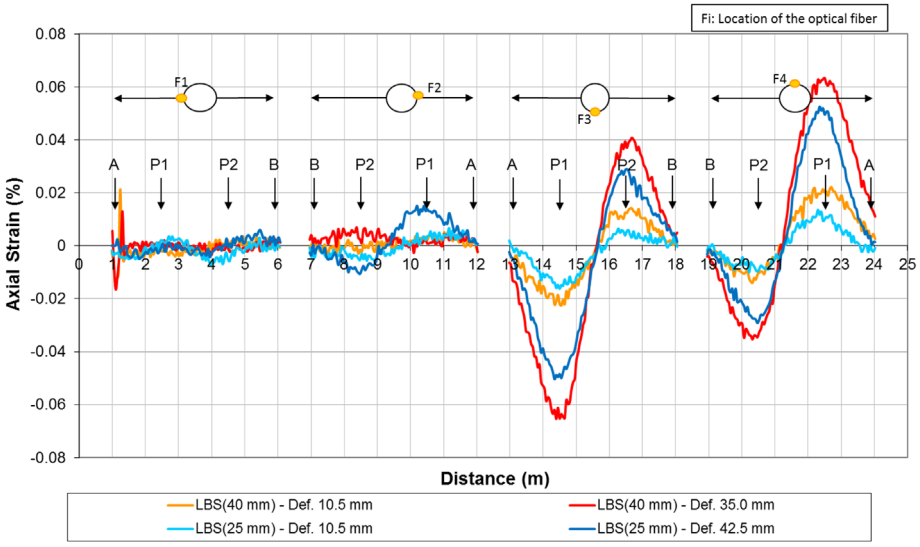

Fig. 12. Comparison of measurements made by test tube with diameter 40 mm and 25 mm (test Type I).

type I: for the same vertical (y direction) displacement of support P1 (10.5 mm), 40 mm diameter ST develops greater axial strain values than the 25 mm diameter ST.

These preliminary measurements are only used to check that the sensor is adequately connected to the receptor equipment located hundred meters away from the measured point. More rigorous testing and comparison with other types of instruments must be performed to guarantee that the proposed sensors are operating properly on the field.

6. Conclusions

In this paper a monitoring system based on a 5 m length 40 mm diameter and 3 mm thickness PVC tube instrumented with optical fiber connected to a Brillouin Optical Time Domain Reflectometer (BOTDR) apparatus is proposed to monitor rock mass displacement due to mining activities. The optical fiber is glued along four lines of the tube surface which are rotated 90 degrees one from each other to capture in-plane and out-of-plane tube displacements in which the sensor has been designed to be attached at four points to tunnel sidewall and ceiling. Laboratory tests were carried out to study the behavior of the sensor tube (ST) as a monitoring tool under different supports (i.e., anchoring points of the sensor) displacements that represent expected deformation within the rock mass. Axial strain values in the range of 0.01–0.1%, that corresponds to a relative supports displacement up to 50 mm, and their distribution along the sensor length measured by the optical fiber were validated by comparisons with electrical resistance strain gauges measurements and results given by a mechanical model that assumes that the sensor behaves as a one-dimensional linear Bernoulli beam element.

A back-analysis algorithm is proposed to estimate rock mass movements (i.e, relative displacements of the sensor supports) from the axial strain values measured by the optical fiber. The ST is modeled as a one-dimensional linear Bernoulli beam element with unknown boundary conditions which are estimated throughout an iterative process that includes the minimization of an error function. This function is based on the difference between the measured axial strain values and the ones predicted for a given boundary condition of the sensor that represents a particular rock mass movement.

The installation procedure of the proposed ST in an underground mine is described and preliminary strain measurements for a period of time equal to 3 months are reported to show that the ST is adequately connected to the receptor equipment located hundred meters away from the measured point. Experimental results and numerical simulations show that the use of PVC tubes with larger diameters to construct the sensors would allow us to better detect (recorded strains greater than the error associated to the optical fiber) small relative displacements between sensors supports induced by rock mass movements. The results of this study along with the fact that BOTDR-based systems allow long distance monitoring, their resistant to high temperature, chemicals, and their immune to electromagnetic interference suggest that the proposed sensor is a promising monitoring tool to detect deformation in tunnels and its use can be extended to other geotechnical application such as measuring failure surfaces and differential settlements below foundations.

Acknowledgments

The experimental work was conducted in collaboration with MICOMO, which provided financial support and supplied the BOTDR equipment used in the program of testing. The advice and support of Mr. Luis Mujica and Ms. Alejandra Alvarez is gratefully appreciated.

References

[1] Kurashima T, Usu T, Tanaka K, Nobiki A. Application of fiber optic distributed sensor for strain measurement in civil engineering. SPIE 1997;3241:247–58.
[2] Ohno H, Naruse H, Kihara M, Shimada A. Industrial applications of BOTDR optical fiber strain sensor. Opt Fiber Technol 2001;7:45–64.
[3] Li H, Li D, Song G. Recent applications of fiber optic sensor to health monitoring in civil engineering. Eng Struct 2004;26:1647–57.
[4] Shen B, King A, Guo H. Displacement, stress and seismicity in roadway roofs during mining-induced failure. Int J Rock Mech Min Sci 2008;45:672–88.
[5] Sayar A, Khalilpasha M. Using extensometer as a monitoring system, case study: Taloun Pilot in Teheran-north of Iran freeway. J Basic Appl Sci Res 2012;2:1696–700.
[6] Shentu N, Zhang H, Li Q, Zhou H, Tong R, Li X. A theoretical model to predict both horizontal displacement and vertical displacement for electromagnetic induction-based deep displacement sensors. Sensors 2012;12:233–59.
[7] Kontogianni V, Tzortzis A, Sitros S. Deformation and failure of the Tymfristos tunnel, Greece. J Geotech Geoenviron Eng 2004;130:1004–13.
[8] Kontogianni V, Sitros S. Induced deformation during tunnel excavation: evidence from geodetic monitoring. Eng Geol 2005;79:115–26.
[9] Kim S, Lee J, Kwon I. Structural monitoring of a bending beam using Brillouin distributed optical fiber sensors. Smart Mater Struct 2002;11:396–403.
[10] Bao X, Webb J, Jackson D. 32-km distributed temperature sensor based on Brillouin loss in an optical fiber. Opt Lett 1993;18:1561–3.

[11] Naruse H, Uehara H, Deguchi T, Fijihashi K, Onishi M, Espinoza R, et al. Application of a distributed fibre optic strain sensing system to monitoring changes in the state of an underground mine. Meas Sci Technol 2007;18: 3202–3210.
[12] Inaudi D, Glisic B. Long-range pipeline monitoring by distributed fiber optic sensing. J Press Vessel Tech 2010;132:1–9.
[13] Glisic B, Yao Y. Fiber optic method for health assessment of pipelines subjected to earthquake-induced ground movement. Struct Health Monit 2012;11: 696–711.
[14] Kurashima T, Usu T, Tanaka K, Nobiki A. Application of fiber optic distributed sensor for strain measurement in civil engineering. SPIE 1997;3241:247–58.
[15] Mohamad H, Soga K, Bennet P, Mair R, Lim C. Monitoring twin tunnel interaction using distributed optical fiber strain measurements. J Geotech Geoenviron Eng 2012;138:957–67.
[16] Gage J, Fratta D, Turner A, Maclaughlin M, Wang H. Validation and implementation of a new method for monitoring in situ strain and temperature in rock masses using fiber-optically instrumented rock strain and temperature strips. Int J Rock Mech Min Sci 2013;61:244–55.
[17] Duratec Vinilit PVC tube property manual ⟨www.vinilit.cl⟩.
[18] Sandoval J. Resolución especial en la aplicación de fibra óptica (BOTDR) en pernos de anclaje de soporte de túneles. ([Master thesis]). Chile: University of Chile; 2010 (in Spanish).
[19] Rodrigues C, Inaudi D, Glisic B. Long-gauge fibre optic sensor: performance comparison and applications. Int J Lifecycle Perform Eng 2013;1:209–33.
[20] Popov E. Engineering mechanics of solids. 2nd ed. New York: Prentice-Hall; 1998.
[21] McGuire W, Gallgher R, Ziemian R. Matrix structural analysis. 2nd ed. New York: Wiley; 2000.
[22] Ling J, Hudson JA. Numerical methods in rocks mechanics. Int J Rock Mech Min Sci 2002;39:409–27.
[23] Ling J. A review of techniques advances and outstanding issues in numerical modelling for rock mechanics and rock engineering. Int J Rock Mech Min Sci 2003;40:283–353.
[24] Sotomayor J. Plataforma computacional para el análisis de un sensor de desplazamientos en túneles. ([thesis civil engineering]). Chile: University of Chile; 2013 (in Spanish).